Acta Materialia 165 (2019) 118–128

Contents lists available at ScienceDirect

Acta Materialia

journal homepage: www.elsevier.com/locate/actamat

Full length article

Unprecedented irradiation resistance of nanocrystalline tungsten with equiaxed nanocrystalline grains to dislocation loop accumulation

O. El-Atwani [a, *], E. Esquivel [a], E. Aydogan [a], E. Martinez [a], J.K. Baldwin [c], M. Li [b], B.P. Uberuaga [a], S.A. Maloy [a]

[a] Materials Science and Technology Division, Los Alamos National Laboratory, Los Alamos, NM, USA
[b] Division of Nuclear Engineering, Argonne National Laboratory, Argonne, IL, USA
[c] Center for Integrated Nanotechnology, Los Alamos National Laboratory, Los Alamos, NM, USA

ARTICLE INFO

Article history:
Received 18 September 2018
Received in revised form
23 October 2018
Accepted 12 November 2018
Available online 15 November 2018

Keywords:
Nanocrystalline
In-situ TEM
Grain boundaries
Dislocation loops

ABSTRACT

Nanocrystalline metals are often postulated as irradiation tolerant materials due to higher grain boundary densities. The efficiency of these materials in mitigating irradiation damage is still under investigation. Here, we present an in-situ transmission electron microscopy with ion irradiation study on equiaxed 35 nm grained tungsten (NCW-35 nm) and compare its radiation tolerance, in terms of dislocation loop damage, to several other grades of tungsten with different grain sizes at two temperatures (RT and 1073 K). The NCW-35 nm was shown to possess significant higher radiation tolerance in terms of loop damage. As demonstrated by Kinetic Monte Carlo simulations, at least part of the higher radiation tolerance of the small grains is due to higher interstitial storage (at the grain boundaries) and defect recombination (in the grain interiors) in the small grain material. In addition, experimental observations reveal rapid and efficient dislocation loop absorption by the grain boundaries and this is considered the dominant factor for mass transport to the boundaries during irradiation, enabling the remarkable radiation tolerance of 35 nm grained tungsten. This study demonstrates the possibility of attaining high radiation tolerant materials, in terms of dislocation loop damage, by minimizing grain sizes in the nanocrystalline regime.

Published by Elsevier Ltd on behalf of Acta Materialia Inc.

1. Introduction

Novel materials that can sustain harsh irradiation environments are sought for upcoming nuclear power systems. Both next generation fusion and fission reactors require materials of exceptional performance in terms of resistance to the microstructural damage and the consequent mechanical properties degradation when exposed to neutron or plasma irradiation [1–8]. Current research is focused on the discovery of new materials or the alteration of existing materials to sustain high doses of radiation [9,10]. Metallic multilayers [11–13], high entropy alloys [14,15], nanotwinned metals [16–18], nanovoided [16] or nonporous metals [19], complex oxides [20,21] and nanocrystalline metals and ceramics [22–27] are among the novel materials that are being examined. Some of these engineered materials have shown high performance under extreme irradiation environments [16,18] but their use in future reactors requires further study either because other reactor operation factors should be considered or their industrial design is a challenge [28]. Alteration of existing and previously tested materials can then be a more efficient solution. Nanocrystalline materials of high grain boundary density are considered high radiation resistant materials as the grain boundaries play the role of neutral sinks for irradiation generated defects [24,29–32]. Moreover, these materials possess enhanced mechanical properties [33–38]. The improvement introduced by some nanocrystalline materials in terms of radiation resistance was not large [39], and their efficiency was shown to depend on the grain boundary microscopic character [24,40–43]. Some recent work, however, has suggested radiation resistance dependence on the grain size in the nanocrystalline regime (˂ 100 nm) [23,39,44].

Here, we examine equiaxed nanocrystalline pure tungsten with grain sizes ≤35 nm, a size regime that has not been previously examined in tungsten, under heavy ion irradiation (Kr^{+2}) in-situ in a transmission electron microscope (TEM) under low (RT) and high (1073 K) temperature conditions. In addition to the high thermal

* Corresponding author.
E-mail addresses: oelatwan25@gmail.com, osman@lanl.gov (O. El-Atwani).

https://doi.org/10.1016/j.actamat.2018.11.024
1359-6454/Published by Elsevier Ltd on behalf of Acta Materialia Inc.

stability prior and during irradiation, the material demonstrated unprecedented high radiation resistance as compared to larger grain size nanocrystalline material and to a conventional material (coarse grained). The in-situ nature of the experiments permitted the visualization of fast and high efficient absorption of defect clusters by grain boundaries and the evolution of damage as a function of radiation dose. Kinetic Monte Carlo simulations confirmed the dependence of radiation resistance on grain size in the nanocrystalline regime. Due to the extremely small grain size, this material is of extraordinary resistance regardless of the grain boundary character. This study provides new insight on the design of extreme radiation resistant nanocrystalline materials and highlights the size regimes in which they should be investigated.

2. Experimental

2.1. Sample synthesis and preparation

TEM sample preparation of the NCW films was performed by floating the film (prepared on NaCl salt) on a standard molybdenum TEM grid using 1:1 ethanol/water solution [45]. The films were prepared via magnetron deposition from a tungsten target of 99.99% purity. The deposition was performed at RT using 100 Watts DC power and 4mTorr pressure. To achieve a 100 nm thickness, ~280 s of deposition time was required. The grain size can vary with small changes in temperature during deposition. TEM sample preparation of the SPD (prepared through orthogonal machining process [46]) and the CWG (purchased from ESPI Metals, US) were prepared by mechanical polishing the samples to 100 μm thickness before electropolishing with 0.5% NaOH solution at RT a final step. The films as well as the electropolished-thin area in the SPD and the CGW samples were ~100 nm thickness. The thicknesses of the films were measured using cross-section FIB imaging.

2.2. In-situ Kr ion irradiation

In-situ Kr^{+2} ion irradiation with 1 MeV was performed using the intermediate voltage electron microscope (IVEM) attached to a Tandem accelerator at Argonne National Laboratory. The electron beam energy was 300 kV and the average dose rate was 0.00075 dpa.s^{-1} throughout the experiment for the samples irradiated to a final dose of 2 dpa and 0.002 dpa.s^{-1} throughout the experiment for the sample irradiated to a final dose of 10 dpa. We do not expect an effect of the different dpa rate (factor of 2.8) on the damage observed. The experiments were performed at RT and 1073 K. A CCD camera with 4kx4k resolution was used to capture the video and still images at different dpa values. The dpa values were calculated (see Supplementary Fig. S1) using the Kinchin-Peace model in the Stopping Range of Ions in Matter (SRIM) Monte Carlo computer code (version 2013) [47] and 40 eV [48] was taken as the displacement threshold energy. Prior to the in-situ experiment, the samples were annealed in-situ inside the TEM using a Gatan Heating holder at 1123 K. The in-situ experiments were performed on grains that did not possess pre-irradiation dislocation density.

2.3. Analysis

Analysis of loop densities was performed by counting the number of loops and dividing the result by the area of the grain measured using Image J software. All grains quantified were chosen to be in multibeam conditions to capture the total loop density. For void damage, Fresnel under-focused images are analyzed. All images were taken under the same under-focus value (1.5 μm) to compare void damage between the different grades. Details about the analysis processes and examples can be found in Ref. [44] and ref. [49].

2.4. Kinetic Monte Carlo simulations

The kinetic Monte Carlo (KMC) [50–52] algorithm solves the dynamic evolution of a Markovian process provided that the probabilities per unit time of the possible events are first order in time and they are known. It has been extensively used to study radiation damage, following the irradiation-induced defects as they are formed and diffuse in system [53] (and references therein). In our model, vacancies (V) and self-interstitials (SI) are created at a given dose rate. They can diffuse on an underlying lattice with a rate calculated via harmonic transition state theory [54] knowing the migration barrier and with a constant pre-factor equal to 10^{12} s^{-1}. Vacancies and SIs can recombine if they are at a first nearest neighbor (1nn) distance. Interfaces are model as regions in the system where defects have different thermodynamic and kinetic properties. In the case of W, the migration barrier in bulk was $\Delta E^{V}_{bulk} = 1.667$ eV and $\Delta E^{SI}_{bulk} = 0.054$ eV for V and SIs, respectively [55,56]. Dose rates, binding energies to the interface, migration energies at the interface and temperature were varied to test different hypothesis.

3. Results

Four different materials were investigated: 1) Nanocrystalline tungsten (NCW) prepared through magnetron deposition with an average grain size of ~35 nm, labelled as NCW-35 nm; 2) NCW prepared through magnetron deposition with an average grain size of ~85 nm, labelled as NCW-85 nm; 3) Nanocrystalline and ultrafine tungsten (where both nanocrystalline grains of sizes less than 100 nm and ultrafine grains of sizes, 100–500 nm co-exist) prepared through severe plastic deformation method (orthogonal machining), labelled as SPD; and 4) Coarse-grained tungsten with grains of average size of 1–3 μm, purchased through ESPI Metals, USA and labelled as CGW. The irradiation conditions of every tungsten grade are summarized in Table 1.

Fig. 1 shows bright-field TEM images of the same specimen area of unirradiated tungsten grades (prior to the experiment) and of the materials irradiated to several displacements-per-atom (dpa) values. For the two NCW specimens, post irradiated TEM images (taken 1 week after the in-situ experiment where the sample was held at ambient conditions) are also shown, which reveal the continued defect evolution in the sample cooling phase and during sample storage at ambient. For the SPD and the CGW, the increase in damage vs dpa is clear. For the NCW specimens, while the damage increases for low dpa, it saturates at a low dose, and remains constant and relatively low, upon further irradiation. These images suggest that the nanocrystalline materials exhibit better radiation tolerance than the larger grained materials.

The damage in the samples is quantified by examining the density and size of dislocation loops (both interstitial and vacancy type) in the material, as shown in Fig. 2 (uncertainties in the values were 10% for the loop density and area and 14% for the total

Table 1
Irradiation conditions and average grain sizes of the different tungsten grades in this work.

Tungsten Grade	Average Grain Size	Temperature	Final Dose (dpa)
CGW	1–3 μm	1073 K	2
SPD	80–400 nm	RT&1073 K	2 (RT & 1073K)
NCW-85 nm	85	1073 K	2
NCW-35 nm	35	RT&1073 K	2 (RT) & 10 (1073K)

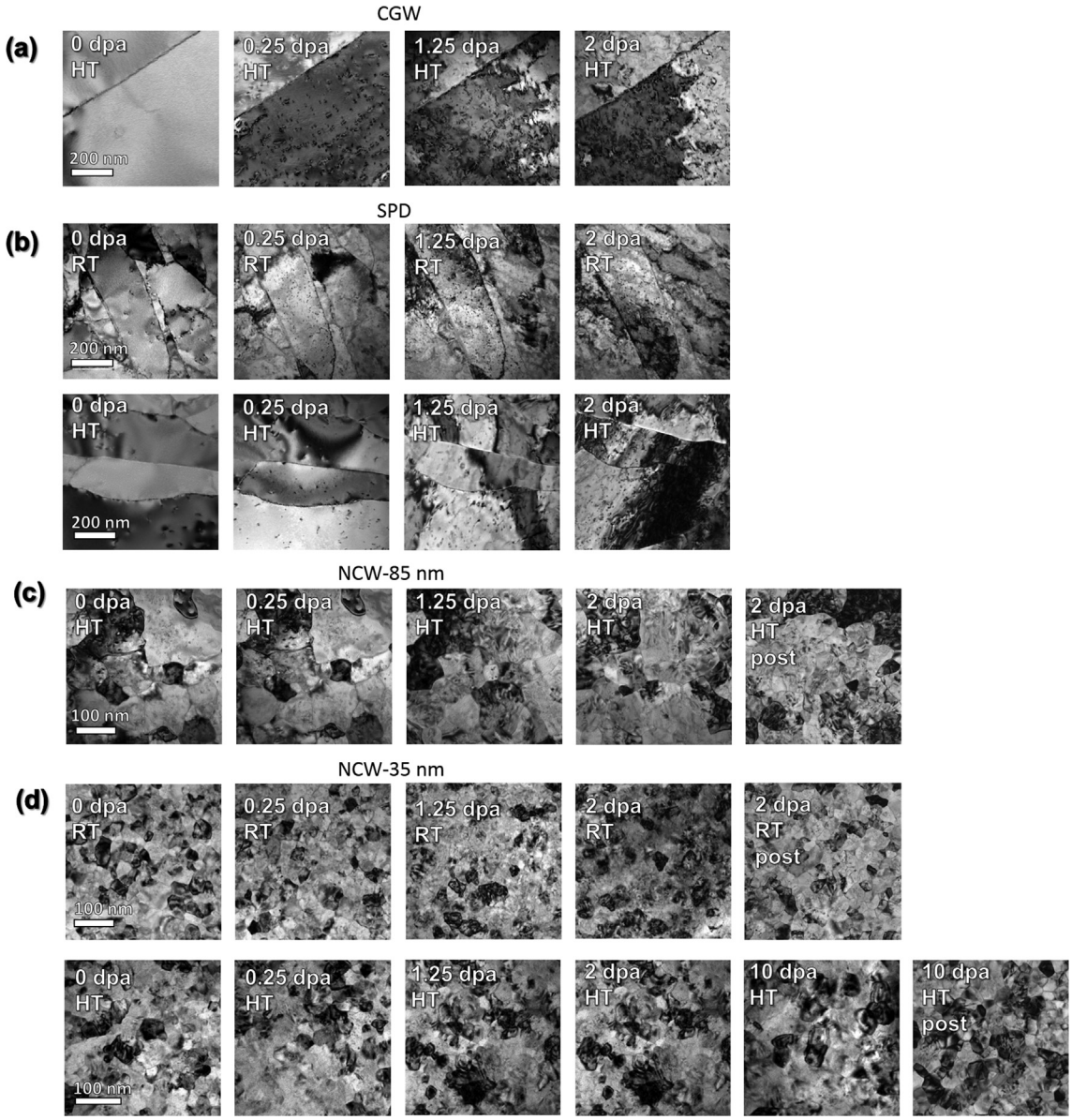

Fig. 1. Bright-field TEM micrographs of the unirradiated and irradiated tungsten grades as a function of dpa. (a) CGW, (b) SPD, (c) NCW-85 nm and (d) NCW-35 nm. In the case of the two NCW films, post-examination images are also shown.

damage). Loop areal densities, average loop area and the overall damage (product of loop density and average loop area) are shown as a function of dpa in a TEM foil with a thickness of ~100 nm. Starting with the largest grain size grade (CGW), at 1073 k, the loop density saturates after ~ 0.5 dpa at a value of 0.004 (no.nm^{-2}), while loop area increases consistently until the final dose of 2 dpa, reaching a value of about 140–150 nm^2. The increase in loop area at fixed loop density suggests an increase in defect accumulation to the loops and a suppression of the nucleation of new loops. No loop coalescence occurred since no decrease in loop density has been observed. The overall damage (product of loop density and average area) was ~0.8 at 2 dpa.

For the SPD (grain sizes of 80–400 nm), the experiments were performed at both RT and 1073 K and quantifications were made from grains of ~200 nm grain size. At RT, the loop density increases with dpa up to 1 dpa and then starts to scatter around 0.009 (no.nm^{-2}), while the loop areas show very little increase with dpa, saturating at a value of ~20 nm^2. At 1073 K, a similar trend is observed but the loop density saturates at about half the value (~0.0045 no.nm^{-2}) seen at RT while the average loop area saturates at about 50 nm^2. The overall damage at 1073 K is perhaps slightly smaller than at RT but in both cases the total damage at 2 dpa scatters around 0.2. In neither case do we observe either loop density decrease or a large increase in loop area, suggesting no loop coalescence. At 1073 K, the loop density is lower but the loop area is higher than the RT case, suggesting competing effects that cancel, resulting in similar overall damage. Moreover, the overall damage is about four times smaller in the SPD than in the CGW at 1073 K.

For the NCW-85 nm film (average grain size of ~85 nm), one experiment was performed at 1073 K. Both loop density and loop area exhibit flat profiles starting from a dose of 0.2 dpa. The saturated loop density is ~0.002 (no.nm-2) while the average loop area is ~20–30 nm^2. The overall damage is about 0.2. Post examination of the sample (1 week after the in-situ experiment where the sample was held at ambient conditions) revealed much lower values (about 20 times smaller, shown in Fig. 2 (c)) of loop density,

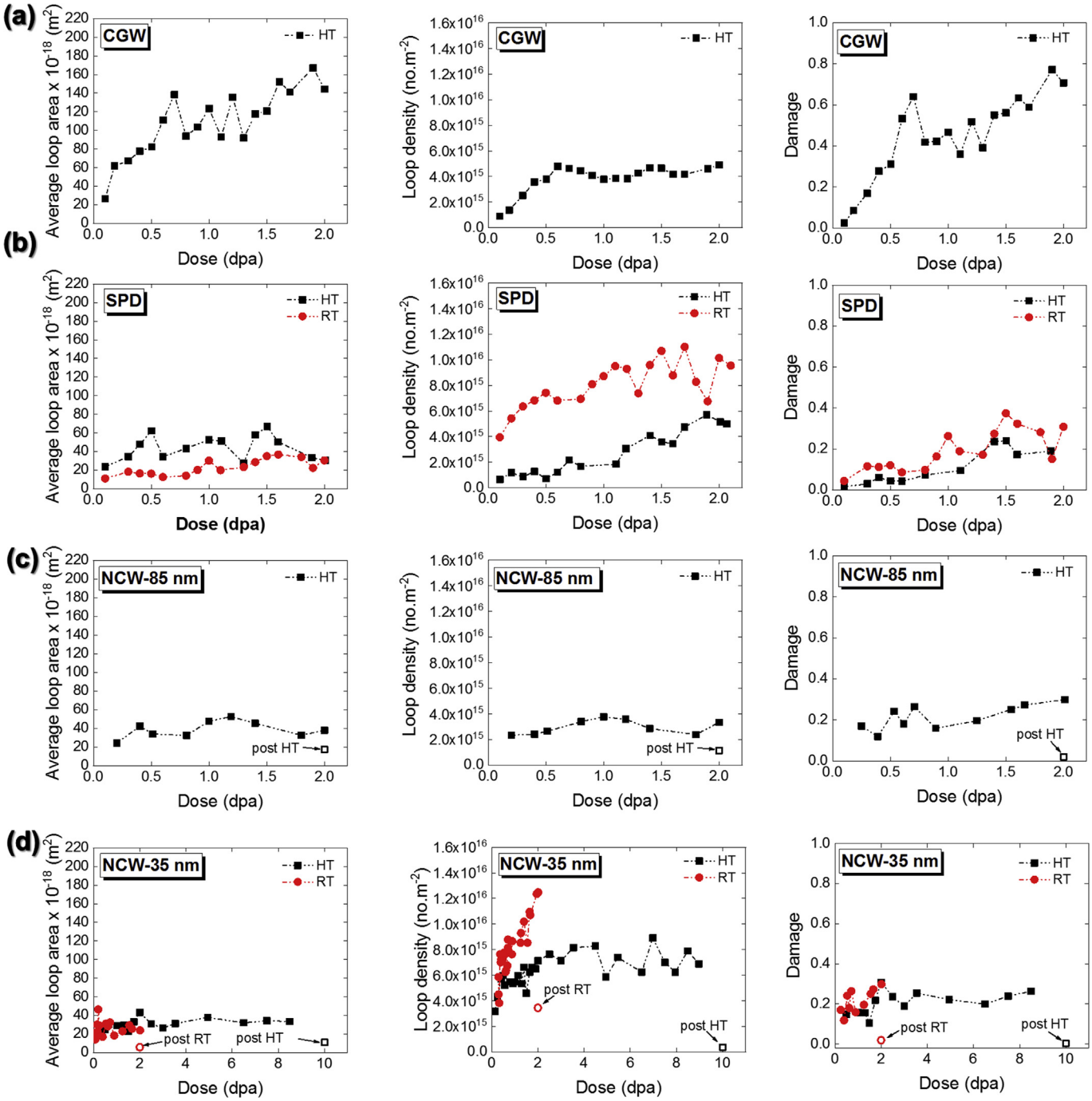

Fig. 2. Three measures of loop damage in the irradiated samples – areal loop densities, average loop areas and total damage (product of areal loop density and average loop areas) – as a function of dpa and temperature (in the case of SPD and NCW-35 nm). Loop area and density values have 10% uncertainty while total damage values have 14% uncertainty.

average loop area and overall damage. It should be mentioned that for Cu^{+} (3 MeV) irradiated SPD samples [49], higher total damage (considering the product of loop density and average area) is observed at high temperature than RT (opposite to this work) which can be attributed to collision cascade effects of Kr versus Cu and different grain boundary sink efficiencies of the different grains quantified.

Finally, for the NCW-35 nm film (average grain size of ~35 nm), the experiment was performed at RT and 1073 K. For the higher temperature, the experiment was continued to 10 dpa. At RT, an increase in loop density vs dpa occurs (~0.012 at 2 dpa), while the loop area profile is constant versus dpa (~20 nm^2). The overall damage is 0.2 at the start of the experiment and increases to 0.3 at 2 dpa. At 1073 K, the loop density increases to 0.006 at 0.25 dpa and fluctuates around that value through to the highest dose (10 dpa). The average loop area is about 30 nm^2 and the overall damage was ~0.2 after 10 dpa. Similar to the NCW-85 nm samples, the post examination values are much smaller (again, after 1 week at ambient conditions). The overall damage is ~20 times less at both RT and 1073 K (even after 10 dpa irradiation). Post-examination of the CGW and the SPD samples did not reveal any change in the microstructure when compared to that observed at the end dose at

the temperature of the in-situ experiments, indicating that the damaged microstructures in those cases is much more stable.

In quantifying the damage in the NCW specimens, grains with contrast under multibeam conditions were chosen. However, to illustrate the effect of diffraction conditions, a post-examined sample (the 1073 K, NCW-35 nm) was tilted in the TEM to different angles (Fig. 3), maintaining focus on the same region of the irradiated sample. The damage is consistent and no effect of diffraction condition was observed on damage quantification.

Table 2
Grain boundary (GB) to surface ratios of the different tungsten grades in this work.

Tungsten Grade	GB/surface
CGW	0.04
SPD	0.47
NCW-85 nm	3.8
NCW-35 nm	7.9

4. Discussion

At 1073 k, vacancies are mobile in tungsten [57], meaning that vacancies can reach interfaces or form voids (by coalescing or feeding vacancy loops), reducing the probability of recombination with interstitials. At RT, however, vacancies are essentially immobile and saturate the irradiation region. Thus, an interstitial has a relatively high probability to recombine with a vacancy when migrating in the sample. That is, interstitial-vacancy recombination is higher when vacancies are dispersed than when they are segregated to loops, voids, or interfaces. Therefore, it is not trivial to compare interstitial-vacancy recombination at RT and 1073 K. The lower density of loops in the cases of SPD, at 1073 K can be related to enhanced loops annihilation by surfaces or interfaces. The total damage originated from loops is not representative by the loop density in this work at 1073 K, if voids are grown from vacancy type loops [49,58].

The NCW films showed similar total damage to the SPD sample (which consists of elongated ultrafine and nanocrystalline grains). This suggests that the actual damage retained in the NCW materials is much lower, due to the following reasons. Irradiation of thin foils is accompanied with surface effects [59]. Surfaces act as tremendous sinks for both point defects (interstitials and vacancies) as well as defect clusters (e.g. loops). The smaller the grain-boundary-area-to-surface-area ratio, the larger the surface effects are. This ratio (considering the upper and low surfaces of the foils) was calculated from TEM micrographs (thickness of the samples is ~100 nm) and are summarized in Table 2.

The grain boundar (GB)/surface ratio of the NCW-35 nm and the NCW-85 nm are about 17 times and 8 times larger than the case of the SPD, respectively. Therefore, it is expected that surfaces play a much larger role in the SPD sample. Therefore, the similar quantified overall damage (Fig. 2) indicates that the NCW samples are of higher radiation tolerance than the SPD sample, as surface effects are minimized in these samples. That is, there is an extra, artificial sink in the CGW and SPD samples that assist defect annihilation that would not be present in a bulk material. Compared to the CGW, where the surface effects are even greater, these samples have ~200 and 100 times larger ratios and, therefore, it can be concluded from Fig. 2 that the NCW samples are of greater radiation tolerance than coarse grained tungsten even when the tremendous surface effects in the coarse grained samples are active. Moreover, the post-examination of the NCW samples revealed at least one order of magnitude lower overall damage than the in-situ values due to efficient loop absorption by the grain boundaries (discussed below). This effect is absent in the CGW and SPD samples.

The similar damage values from the RT and 1073 K experiments indicate similar final loop damage is possible when void growth from vacancy loops is neglected. That is, if only loops are considered, the damage structure is independent of temperature and thus the mobility of vacancies. However, there is more void damage in the higher temperature samples. Thus, in terms of the effect of radiation damage on mechanical properties, samples irradiated at higher temperature should exhibit higher hardening values in the grain matrices (not considering the effects of grain boundaries) than the RT samples due to similar overall loop damage and the presence of void damage which contributes to the hardening of the material [60]. It should be mentioned that the mechanical properties of equiaxed nanocrystalline pure tungsten samples before and after irradiation, where grain boundary mediated plasticity is expected, are still under investigation.

The superiority of the NCW films in terms of radiation tolerance

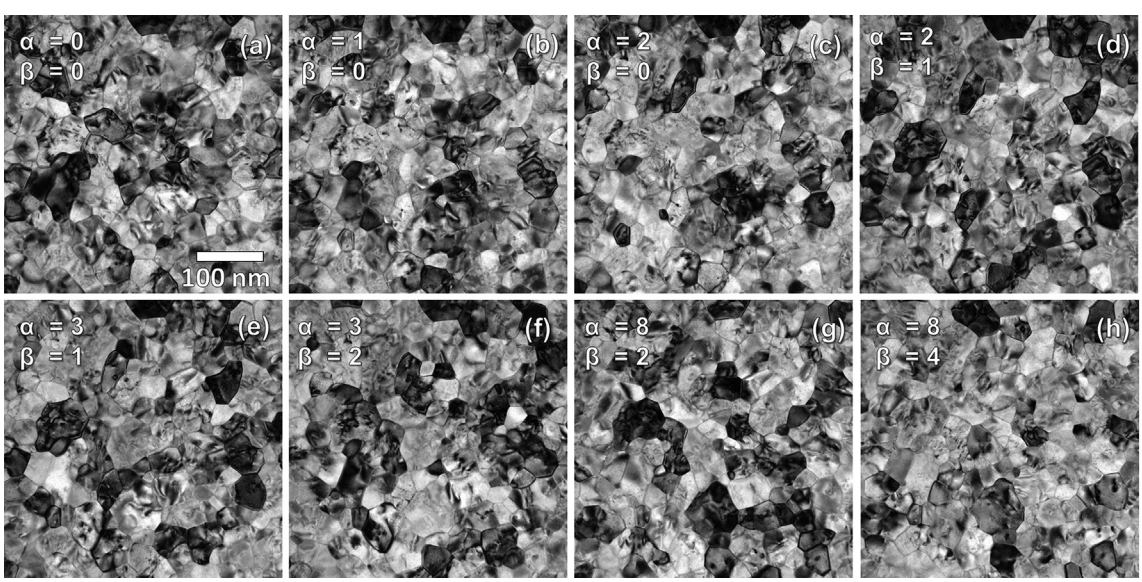

Fig. 3. Bright-field TEM micrographs of post-examined NCW-35nm (10 dpa) with different α and β tilts in the microscope.

to loop damage is mainly due to two reasons. First, the higher grain boundary density provides a mechanism to store interstitials. Second, the observed fast and efficient loop absorption by the grain boundaries provides a mechanism to transport interstitials to grain boundaries. We examine these two effects in more detail in what follows.

4.1. Enhanced interstitial storage and recombination

Fig. 4 shows the average concentration of self-interstitials (SIs) and vacancies in bulk (far from the interface) depending on the grain size, as predicted from KMC simulations. In general, with the model we are using here, for a given production rate, the SI concentration increases as grain sizes increase. This behavior is the result of two effects: the enhanced recombination in small systems due to correlation effects, which is described in the literature [61] and storage of defects at the grain boundary, assuming similar grain boundary properties but the density of interfaces increases. In another study [62], we showed that, even if the sink efficiencies of different boundaries are nearly zero, if they can store a different concentration of interstitials, they will have differing and significant impact on the bulk defect content. This is a simple consequence of the fact that moving defects from the bulk to the boundary reduce the number of defects in bulk. Therefore, we can conclude that the nanocrystalline systems will exhibit improved radiation tolerance even in specific situations in which the grain boundaries are not strong sinks for defects, i.e., when there is a weak recombination probability at the boundary. Fig. 5 shows the self-interstitial concentration profile for the same conditions of irradiation and temperature but different grain sizes. The grain boundary properties are the same in all cases, with equal binding and migration energies of the defects. We observe that for small grain sizes the total number of defects, i.e., the integral of the concentration in the volume, is lower than for larger grains such that $N_{SI}(L) < N_{SI}(nL)/n$, where $N_{SI}(L)$ is the total number of self-interstitials for a given grain length L and n is a factor larger than 1 that accounts for the size increased in larger grains (note that in our simulations we are varying just one dimension). The difference is due to the extra recombination at lower sizes. We also observe that the concentration at the boundary is lower in small grains, which implies that still extra storage can be used in the system to accumulate further defects at the interface. Note also that the concentration at the boundary seems to follow the same form as the bulk concentration, thus the system has not reached saturation yet. To examine the recombination effect in the nanocrystalline grains, void damage was determined and compared between the

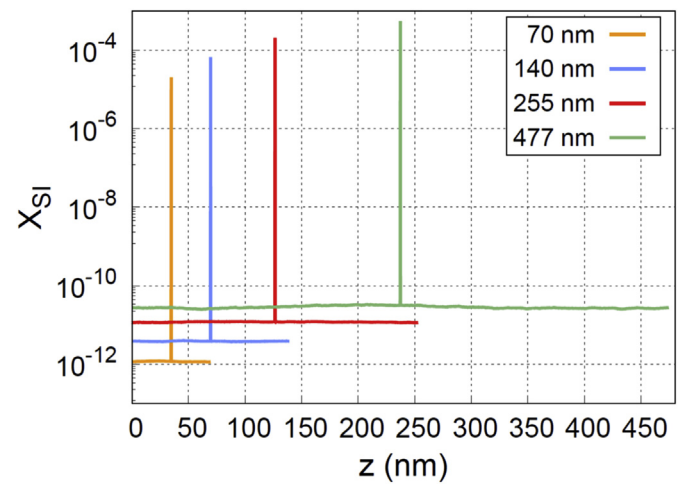

Fig. 5. Concentration profile at 1050 K at steady state for different grain sizes as determined from KMC simulations.

different grades. Fig. 6 shows bright-field Fresnel (under-focused) images of the NCW-85 nm, SPD and CGW which are irradiated to the same dpa at high temperature (1073 K). Void density in the 100 nm film thickness, average void area as well as the total change in volume due to void formation [44] are shown in Fig. 7. The void density in the NCW was higher. The high density of voids in the grain matrices in the NCW is attributed to the less annihilation of small void nuclei due to less interstitials and interstitial loops presence in the grain matrices. The average void area and the corresponding total void damage (change in volume taking into account the void density and average area), however, decrease significantly with the decrease in the grain size indicating less vacancy concentration in the matrices of the NCW in agreement with the simulations results (Fig. 4b). In tungsten, the migration energy of interstitials and vacancies are 0.054 eV and 1.67 eV respectively [55,56], and corresponding mobilities of interstitials and vacancies at 1073 K are 5.6×10^{-4} and 1.65×10^{-11} cm^2/s (the ratio of interstitial mobility to vacancy mobility at 1073 K is approximately 34 million times). Therefore, the vacancy mobility is very low and the decrease in the vacancy concentration in the grain matrices as a function of grain size has to be mainly due to defect recombination. This enhanced recombination at small grain sizes dictated the low void damage in the nanocrystalline grains and ensured extra storage [62] in the grain boundaries.

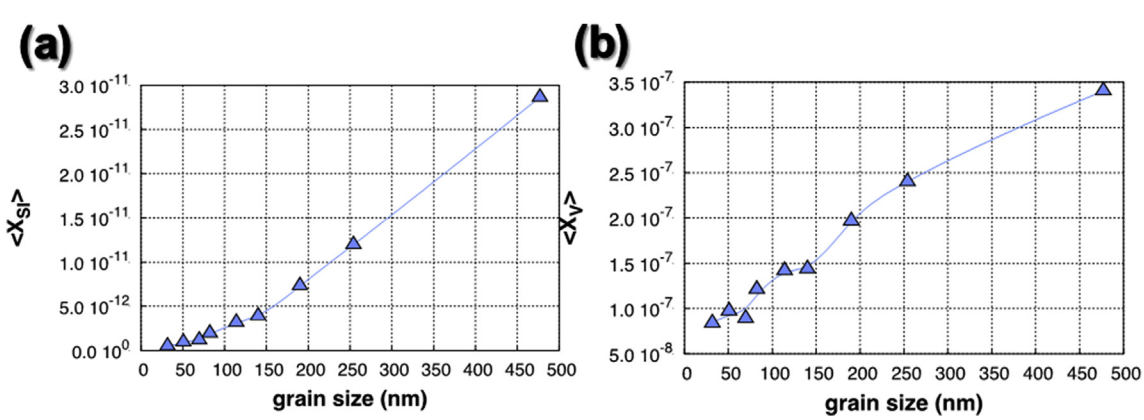

Fig. 4. Average concentration of (a) SI and (b) vacancies in the bulk depending on the grain size of the system. The simulations were performed at 1050 K.

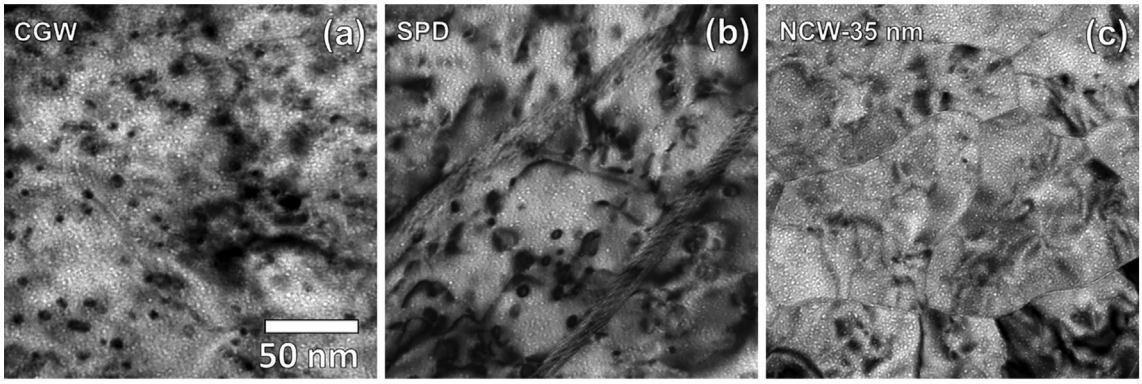

Fig. 6. Under-focused (1.5 μm) bright-field TEM micrographs of post-examined 2 dpa irradiated a) CGW, b) SPD and c) NCW-85 nm 1073 K showing uniform distribution of voids.

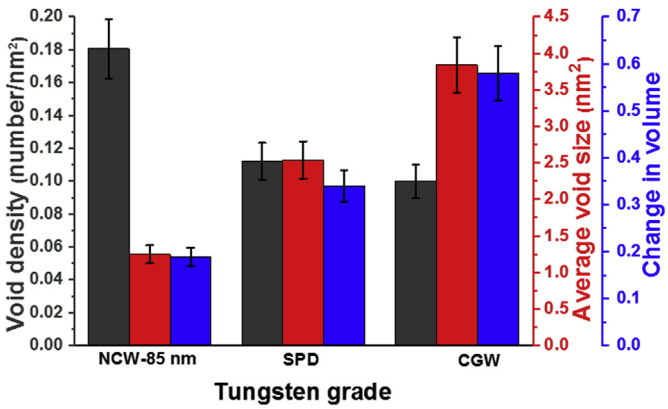

Fig. 7. Void density, average void area and the corresponding change in volume due to void formation in the 1073 K irradiated CGW, SPD and NCW-85 nm at 2 dpa.

4.2. Grain boundary loop absorption

Loop absorption by grain boundaries has been observed in several works [30,31]. In the present study, the NCW-35 nm sample exhibited continuous and rapid loop absorption by the grain boundaries, which could only be observed due to the in-situ nature of the experiments. Fig. 8 (Video S1 in the supplemental materials) shows loop annihilation after nucleation by the grain boundaries. Through this type of process, the sample can maintain a constant density of loops vs time (Fig. 2) when irradiated at RT. Although a similar density of loops is observed in the SPD sample, the much lower GB/surface ratio in the SPD sample results in more loop and defect annihilation by the surfaces, while loops in the NCW-35 nm are absorbed by the grain boundaries. This effect is enhanced at high temperature. At 1073 K, loop absorption occurs more frequently and a higher number of loops are observed to be absorbed by the grain boundaries in a given time period. Fig. 9 (Video S2 in the supplemental materials) shows an example of

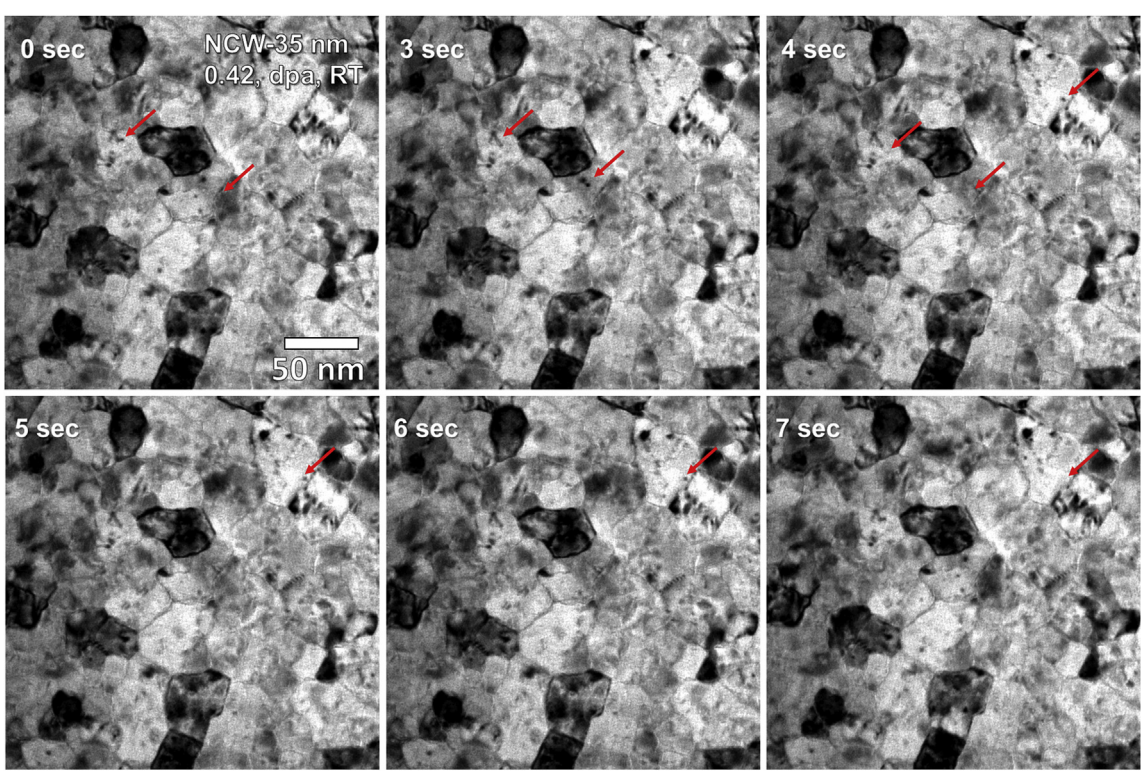

Fig. 8. Snapshots bright-field TEM micrographs taken from an in situ irradiation experiment (Video S1 in the supplemental) at ~ 0.42 dpa showing loop absorption by the grain boundaries in the NCW-35 nm irradiated with 1 MeV Kr^{+2} at RT.

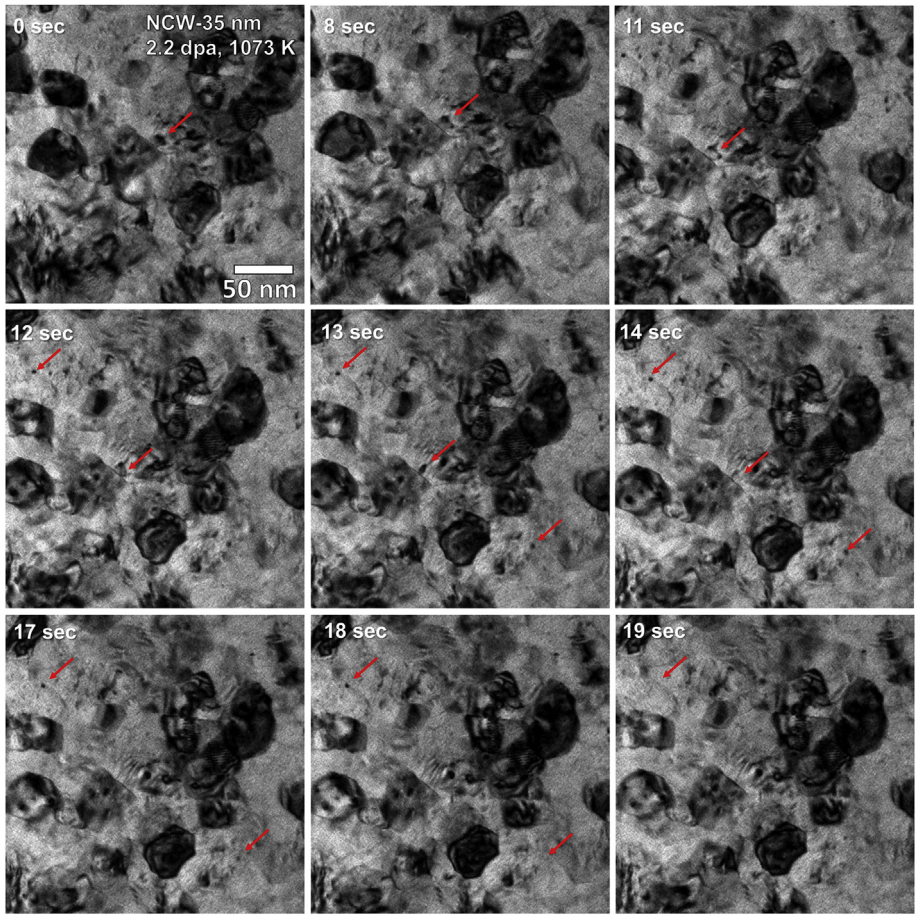

Fig. 9. Snapshots bright-field TEM micrographs taken from an in situ irradiation experiment (Video S2 in the supplemental) at ~2.2 dpa showing loop absorption by the grain boundaries in the NCW-35 nm irradiated with 1 MeV Kr^{+2} at 1073 K.

loop absorption by the grain boundaries at 1073 K. The rapid annihilation by ~35 nm grains at a higher dose is shown in Fig. 10 (Video S3 in the supplemental materials). During 43 s of irradiation time, the number of loops in the 35 nm grains remained the same (1 loop) despite the nucleation of several loops (which were absorbed by GBs after their nucleation). This explains the flat profile in the overall damage (up to 10 dpa) in the NCW-35 nm sample at 1073 K. Post irradiation examination showed an order of magnitude decrease in the damage. After the irradiation stops, loop migration to grain boundaries can continue in the high temperature cases during the temperature ramping down period (where irradiation is stopped). Migration of small loops in tungsten was also shown to occur at RT under the electron beam in the TEM [63]. The loop migration to grain boundaries leads to lower loop densities in the sample. Loop migration will also lead to smaller average loop sizes since the only loops that will remain will be sessile ⟨100⟩ loops (which were concluded to be of vacancy type [64]) and are of much smaller size [49]. This unprecedented amount of loop absorption by the grain boundaries, and the much lower damage of the post examined samples in the 35 nm grains, should be the dominant factor in the extreme radiation tolerance at these grain sizes considering that loops were forming during the irradiation process but were not surviving for a long time before being absorbed by the grain boundaries. However, this efficient loop absorption has to be facilitated by the high recombination in the grain matrices which leaves the grain boundaries of the nanocrystalline grains with extra storage for accumulating further defects (as discussed above).

Supplementary video related to this article can be found at https://doi.org/10.1016/j.actamat.2018.11.024.

Previously [31], in-situ TEM studies were performed on SPD samples at RT, but rare loop absorption by the grain boundaries was observed when compared to the 35 nm grained tungsten, indicating increased jump frequency in the very small grains. For larger grains, interstitial loops can be self-trapped due to interactions with other loops and defects. That is, when loops cannot escape so quickly to interfaces and they build up, the resulting stress fields can enhance trapping of other loops, reducing their rate of absorption. Interaction between loops in tungsten was confirmed experimentally and through modeling approaches, a phenomenon which can ultimately lead to raft formation [63,65,66]. The survival rate of the loops before being annihilated was shown to differ in our samples (Figs. 8–10 and the corresponding videos). We attribute this difference to the efficiency of the grain boundaries and their stress states. It should be mentioned that, in addition to the effect of grain size, the higher stress fields on grain boundaries of the NCW can lead to more efficient absorption of interstitials and interstitial loops by the grain boundaries [67]. However, isolation of the stress field effect is not possible. A future experimental work can focus on in-situ irradiation/straining experiments to examine the effect of grain boundary stress fields on defect absorption. A related observation is that grains with higher stresses (residual stresses from

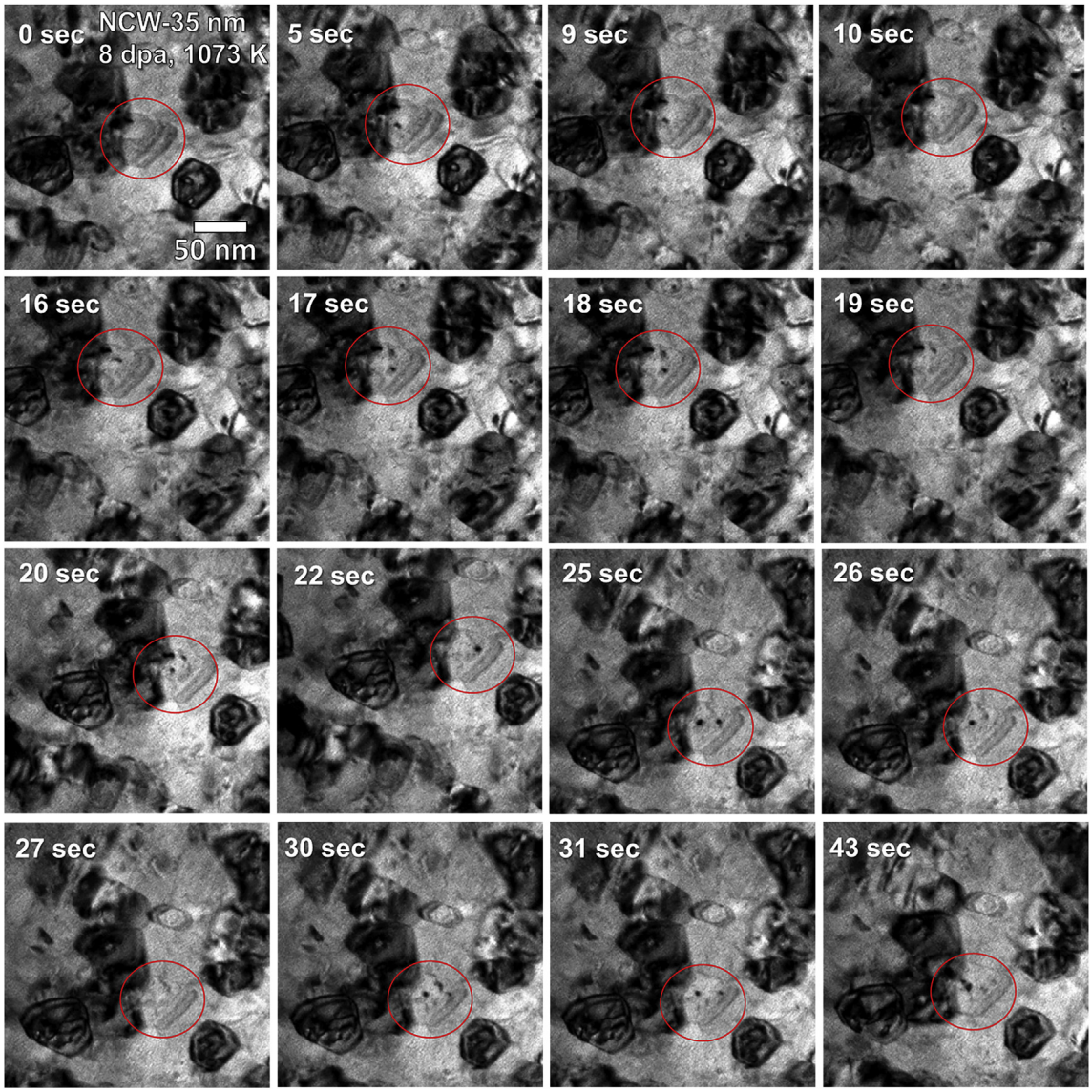

Fig. 10. Snapshots bright-field TEM micrographs taken from an in situ irradiation experiment (Video S3 in the supplemental) at ~ 8 dpa showing loop absorption by the grain boundaries in the same grain in the NCW-35 nm irradiated with 1 MeV Kr^{+2} at 1073 K.

deposition) in the grain matrices (Fig. 11) exhibit higher loop densities. Samara et al. have demonstrated that defect clusters were attracted to regions of large stress gradient [32]. These stresses were noted by dark bending contours in the TEM micrographs. Fig. 8 shows another example of the higher loop density in those grains with larger strains, taken from NCW-85 nm sample. It is, therefore, reasonable to conclude that the density of radiation-induced defects, such as interstitial loops, depends on the strain state of the given grain.

5. Conclusion

In summary, we report a remarkable irradiation tolerance, in terms of dislocation loop damage, of small-grained tungsten when compared to larger grained and coarse grained materials. Dislocation loop densities, average loop sizes and overall loop damage were monitored and quantified in-situ during 1 MeV Kr^{+2} irradiation at RT and 1073 K. Tungsten with grain sizes of 35 nm possesses exceptional radiation tolerance than ultrafine and coarse grained tungsten. These grain sizes also maintain the same overall damage even when irradiated to 5 times higher dpa values than ultrafine and coarse grained tungsten. KMC simulations reveal that nanocrystalline materials contain a lower interstitial defect concentration within the grain matrices as compared to larger grained material, thus explaining part of their irradiation tolerance. The other major factor in the extreme radiation tolerance of these materials is the rapid and continuous loop absorption by the grain boundaries (low survival rates of loops in the grain matrices). The loop absorption by grain boundaries is also responsible for the enhanced radiation tolerance (decrease in radiation damage) of the post examined samples. Nanostructure tungsten is demonstrated to be a promising material resistant to dislocation loop damage, confirming enhanced radiation resistance of nanocrystalline materials.

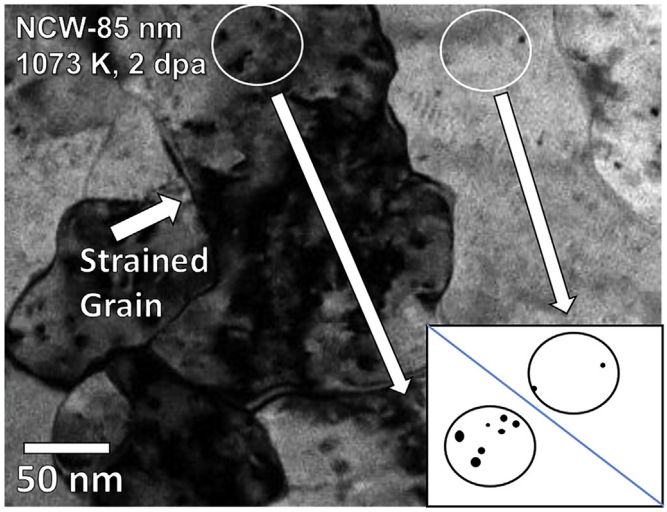

Fig. 11. Bright-field TEM micrograph of irradiated nanocrystalline NCW-85 nm at 1073 K showing grains with higher strain (dark grain) develop more and larger defects (arrows). The inset highlights these defect populations.

Acknowledgements

This work was supported by the U.S. Department of Energy, Office of Nuclear Energy under DOE Idaho Operations Office Contract DE-AC07- 051D14517 as part of a Nuclear Science User Facilities experiment. Research presented in this article was also supported by the Laboratory Directed Research and Development program of Los Alamos National Laboratory under project number 20160674PRD3. We gratefully acknowledge the support of the U.S. Department of Energy through the LANL/LDRD Program and the G. T. Seaborg Institute for this work. B.P.U and E.M acknowledge support by the U.S. Department of Energy, Office of Science, Office of Fusion Energy Sciences, and Office of Advanced Scientific Computing Research through the Scientific Discovery through Advanced Computing (SciDAC) project on Plasma-Surface Interactions under award number DE-SC0008875. The authors would like to thank Peter M. Baldo and Edward A. Ryan for their assistance with the experiments.

Appendix A. Supplementary data

Supplementary data to this article can be found online at https://doi.org/10.1016/j.actamat.2018.11.024.

References

[1] S.J. Zinkle, J.T. Busby, Structural materials for fission & fusion energy, Mater. Today 12 (11) (2009) 12–19.
[2] S.J. Zinkle, G. Was, Materials challenges in nuclear energy, Acta Mater. 61 (3) (2013) 735–758.
[3] R.W. Grimes, R.J. Konings, L. Edwards, Greater tolerance for nuclear materials, Nat. Mater. 7 (9) (2008) 683.
[4] S. Kajita, W. Sakaguchi, N. Ohno, N. Yoshida, T. Saeki, Formation process of tungsten nanostructure by the exposure to helium plasma under fusion relevant plasma conditions, Nucl. Fusion 49 (9) (2009), 095005.
[5] D. Kiener, P. Hosemann, S. Maloy, A. Minor, In situ nano-compression testing of irradiated copper, Nat. Mater. 10 (8) (2011) 608.
[6] C. Cawthorne, E. Fulton, Voids in irradiated stainless steel, Nature 216 (5115) (1967) 575–576.
[7] F. Chu-Chun, J. Dalla Torre, F. Willaime, J.-L. Bocquet, A. Barbu, Multiscale modelling of defect kinetics in irradiated iron, Nat. Mater. 4 (1) (2005) 68.
[8] K. Arakawa, K. Ono, M. Isshiki, K. Mimura, M. Uchikoshi, H. Mori, Observation of the one-dimensional diffusion of nanometer-sized dislocation loops, Science 318 (5852) (2007) 956–959.
[9] G. Ackland, Controlling radiation damage, Science 327 (5973) (2010) 1587–1588.
[10] S.J. Zinkle, L.L. Snead, Designing radiation resistance in materials for fusion energy, Annu. Rev. Mater. Res. 44 (2014) 241–267.
[11] M.J. Demkowicz, R.G. Hoagland, J.P. Hirth, Interface structure and radiation damage resistance in Cu-Nb multilayer nanocomposites, Phys. Rev. Lett. 100 (13) (2008) 136102.
[12] M. Zhernenkov, S. Gill, V. Stanic, E. DiMasi, K. Kisslinger, J.K. Baldwin, A. Misra, M. Demkowicz, L. Ecker, Design of radiation resistant metallic multilayers for advanced nuclear systems, Appl. Phys. Lett. 104 (24) (2014) 241906.
[13] W. Han, M.J. Demkowicz, N.A. Mara, E. Fu, S. Sinha, A.D. Rollett, Y. Wang, J.S. Carpenter, I.J. Beyerlein, A. Misra, Design of radiation tolerant materials via interface engineering, Adv. Mater. 25 (48) (2013) 6975–6979.
[14] J.W. Yeh, S.K. Chen, S.J. Lin, J.Y. Gan, T.S. Chin, T.T. Shun, C.H. Tsau, S.Y. Chang, Nanostructured high-entropy alloys with multiple principal elements: novel alloy design concepts and outcomes, Adv. Eng. Mater. 6 (5) (2004) 299–303.
[15] M.-H. Tsai, J.-W. Yeh, High-entropy alloys: a critical review, Materials Research Letters 2 (3) (2014) 107–123.
[16] Y. Chen, K.Y. Yu, Y. Liu, S. Shao, H. Wang, M. Kirk, J. Wang, X. Zhang, Damage-tolerant nanotwinned metals with nanovoids under radiation environments, Nat. Commun. 6 (2015).
[17] J. Li, K. Yu, Y. Chen, M. Song, H. Wang, M. Kirk, M. Li, X. Zhang, In situ study of defect migration kinetics and self-healing of twin boundaries in heavy ion irradiated nanotwinned metals, Nano Lett. 15 (5) (2015) 2922–2927.
[18] K. Yu, D. Bufford, C. Sun, Y. Liu, H. Wang, M. Kirk, M. Li, X. Zhang, Removal of stacking-fault tetrahedra by twin boundaries in nanotwinned metals, Nat. Commun. 4 (2013) 1377.
[19] E.M. Bringa, J. Monk, A. Caro, A. Misra, L. Zepeda-Ruiz, M. Duchaineau, F. Abraham, M. Nastasi, S. Picraux, Y. Wang, Are nanoporous materials radiation resistant? Nano Lett. 12 (7) (2011) 3351–3355.
[20] K.E. Sickafus, R.W. Grimes, J.A. Valdez, A. Cleave, M. Tang, M. Ishimaru, S.M. Corish, C.R. Stanek, B.P. Uberuaga, Radiation-induced amorphization resistance and radiation tolerance in structurally related oxides, Nat. Mater. 6 (3) (2007) 217.
[21] K. Sickafus, L. Minervini, R. Grimes, J. Valdez, M. Ishimaru, F. Li, K. McClellan, T. Hartmann, Radiation tolerance of complex oxides, Science 289 (5480) (2000) 748–751.
[22] I. Beyerlein, A. Caro, M. Demkowicz, N. Mara, A. Misra, B. Uberuaga, Radiation damage tolerant nanomaterials, Mater. Today 16 (11) (2013) 443–449.
[23] O. El-Atwani, J. Hinks, G. Greaves, S. Gonderman, T. Qiu, M. Efe, J. Allain, In-situ TEM observation of the response of ultrafine-and nanocrystalline-grained tungsten to extreme irradiation environments, Sci. Rep. 4 (2014).
[24] I. Beyerlein, M. Demkowicz, A. Misra, B. Uberuaga, Defect-interface interactions, Prog. Mater. Sci. 74 (2015) 125–210.
[25] X.-M. Bai, A.F. Voter, R.G. Hoagland, M. Nastasi, B.P. Uberuaga, Efficient annealing of radiation damage near grain boundaries via interstitial emission, Science 327 (5973) (2010) 1631–1634.
[26] A. Kilmametov, D. Gunderov, R. Valiev, A.G. Balogh, H. Hahn, Enhanced ion irradiation resistance of bulk nanocrystalline TiNi alloy, Scripta Mater. 59 (10) (2008) 1027–1030.
[27] T.D. Shen, S. Feng, M. Tang, J.A. Valdez, Y. Wang, K.E. Sickafus, Enhanced radiation tolerance in nanocrystalline MgGa 2 O 4, Appl. Phys. Lett. 90 (26) (2007), 263115-263115-3.
[28] C.C. Koch, Nanostructured Materials: Processing, Properties and Applications, William Andrew, 2006.
[29] M.A. Tschopp, K. Solanki, F. Gao, X. Sun, M.A. Khaleel, M. Horstemeyer, Probing grain boundary sink strength at the nanoscale: energetics and length scales of vacancy and interstitial absorption by grain boundaries in α-Fe, Phys. Rev. B 85 (6) (2012), 064108.
[30] C. Sun, M. Song, K. Yu, Y. Chen, M. Kirk, M. Li, H. Wang, X. Zhang, In situ evidence of defect cluster Absorption by grain boundaries in Kr ion irradiated nanocrystalline Ni, Metall. Mater. Trans. 44 (4) (2013) 1966–1974.
[31] O. El-Atwani, A. Suslova, T. Novakowski, K. Hattar, M. Efe, S. Harilal, A. Hassanein, In-situ TEM/heavy ion irradiation on ultrafine-and nanocrystalline-grained tungsten: effect of 3MeV Si, Cu and W ions, Mater. Char. 99 (2015) 68–76.
[32] M. Samaras, P. Derlet, H. Van Swygenhoven, M. Victoria, Computer simulation of displacement cascades in nanocrystalline Ni, Phys. Rev. Lett. 88 (12) (2002) 125505.
[33] M.A. Meyers, A. Mishra, D.J. Benson, Mechanical properties of nanocrystalline materials, Prog. Mater. Sci. 51 (4) (2006) 427–556.
[34] R. Valiev, Nanostructuring of metals by severe plastic deformation for advanced properties, Nat. Mater. 3 (8) (2004) 511.
[35] Y. Wang, M. Chen, F. Zhou, E. Ma, High tensile ductility in a nanostructured metal, Nature 419 (6910) (2002) 912–915.
[36] R. Valiev, Materials science: nanomaterial advantage, Nature 419 (6910) (2002) 887–889.
[37] Q. Wei, H. Zhang, B. Schuster, K. Ramesh, R. Valiev, L. Kecskes, R. Dowding, L. Magness, K. Cho, Microstructure and mechanical properties of super-strong nanocrystalline tungsten processed by high-pressure torsion, Acta Mater. 54 (15) (2006) 4079–4089.
[38] Q. Wei, T. Jiao, K. Ramesh, E. Ma, L. Kecskes, L. Magness, R. Dowding, V. Kazykhanov, R. Valiev, Mechanical behavior and dynamic failure of high-strength ultrafine grained tungsten under uniaxial compression, Acta Mater. 54 (1) (2006) 77–87.
[39] O. El-Atwani, J. Nathaniel, A. Leff, K. Hattar, M. Taheri, Direct observation of sink-dependent defect evolution in nanocrystalline iron under irradiation, Sci.

Rep. 7 (2017).
[40] C.M. Barr, G.A. Vetterick, K.A. Unocic, K. Hattar, X.-M. Bai, M.L. Taheri, Anisotropic radiation-induced segregation in 316L austenitic stainless steel with grain boundary character, Acta Mater. 67 (2014) 145–155.
[41] X.-M. Bai, L.J. Vernon, R.G. Hoagland, A.F. Voter, M. Nastasi, B.P. Uberuaga, Role of atomic structure on grain boundary-defect interactions in Cu, Phys. Rev. B 85 (21) (2012) 214103.
[42] B.P. Uberuaga, L.J. Vernon, E. Martinez, A.F. Voter, The relationship between grain boundary structure, defect mobility, and grain boundary sink efficiency, Sci. Rep. 5 (2015).
[43] A. Dunn, R. Dingreville, E. Martínez, L. Capolungo, Identification of dominant damage accumulation processes at grain boundaries during irradiation in nanocrystalline α-Fe: a statistical study, Acta Mater. 110 (2016) 306–323.
[44] O. El-Atwani, J. Nathaniel, A. Leff, B. Muntifering, J. Baldwin, K. Hattar, M. Taheri, The role of grain size in He bubble formation: implications for swelling resistance, J. Nucl. Mater. 484 (2017) 236–244.
[45] G. Vetterick, J. Baldwin, A. Misra, M. Taheri, Texture evolution in nanocrystalline iron films deposited using biased magnetron sputtering, J. Appl. Phys. 116 (23) (2014) 233503.
[46] M. Efe, O. El-Atwani, Y. Guo, D.R. Klenosky, Microstructure refinement of tungsten by surface deformation for irradiation damage resistance, Scripta Mater. 70 (2014) 31–34.
[47] J.F. Ziegler, M.D. Ziegler, J.P. Biersack, SRIM–The stopping and range of ions in matter, Nucl. Instrum. Methods Phys. Res. Sect. B Beam Interact. Mater. Atoms 268 (11) (2010) 1818–1823, 2010.
[48] P. Jung, in: H. Ullmaier (Ed.), Atomic Defects in Metals (Landolt-bornstein New Series III/25), Springer, Berlin, 1991.
[49] O. El-Atwani, E. Esquivel, M. Efe, E. Aydogan, Y. Wang, E. Martinez, S. Maloy, Loop and void damage during heavy ion irradiation on nanocrystalline and coarse grained tungsten: microstructure, effect of dpa rate, temperature, and grain size, Acta Mater. 149 (2018) 206–219.
[50] E. Elcock, Vacancy diffusion in ordered alloys, Proc. Phys. Soc. 73 (2) (1959) 250.
[51] E.W. Elcock, C.W. McCombie, Phys. Rev. Lett. (1957) 605.
[52] A.B. Bortz, M.H. Kalos, J.L. Lebowitz, A new algorithm for Monte Carlo simulation of Ising spin systems, J. Comput. Phys. 17 (1) (1975) 10–18.
[53] C.S. Becquart, B.D. Wirth, Kinetic Monte Carlo Simulations of Irradiation Effects, Comprehensive Nuclear Materials, Elsevier, London, 2012, p. 3560.
[54] G.H. Vineyard, Frequency factors and isotope effects in solid state rate processes, J. Phys. Chem. Solid. 3 (1–2) (1957) 121–127.
[55] F. Dausinger, H. Schultz, Long-range migration of self-interstitial atoms in tungsten, Phys. Rev. Lett. 35 (26) (1975) 1773.
[56] R.W. Balluffi, Vacancy defect mobilities and binding energies obtained from annealing studies, J. Nucl. Mater. 69 (1978) 240–263.
[57] A. Debelle, M. Barthe, T. Sauvage, First temperature stage evolution of irradiation-induced defects in tungsten studied by positron annihilation spectroscopy, J. Nucl. Mater. 376 (2) (2008) 216–221.
[58] M. Gilbert, S. Dudarev, P. Derlet, D. Pettifor, Structure and metastability of mesoscopic vacancy and interstitial loop defects in iron and tungsten, J. Phys. Condens. Matter 20 (34) (2008) 345214.
[59] M. Li, M. Kirk, P. Baldo, D. Xu, B. Wirth, Study of defect evolution by TEM with in situ ion irradiation and coordinated modeling, Phil. Mag. 92 (16) (2012) 2048–2078.
[60] J.S. Weaver, C. Sun, Y. Wang, S.R. Kalidindi, R.P. Doerner, N.A. Mara, S. Pathak, Quantifying the mechanical effects of He, W and He+ W ion irradiation on tungsten with spherical nanoindentation, J. Mater. Sci. 53 (7) (2018) 5296–5316.
[61] E. Kotomin, V. Kuzovkov, Phenomenological kinetics of Frenkel defect recombination and accumulation in ionic solids, Rep. Prog. Phys. 55 (12) (1992) 2079.
[62] O. El-Atwani, E. Esquivel, M. Efe, C. Taylor, Y.Q. Yang, B.P. Uberuaga, S.A. Maloy, Does Sink Efficiency Unequivocally Characterize How Grain Boundaries Impact Radiation Damage?, Submitted, 2018.
[63] O. El-Atwani, E. Esquivel, M. Efe, Y. Wang, S.A. Maloy, Detailed transmission electron microscopy study on the mechanism of dislocation loop rafting in tungsten, Acta Mater. 147 (2018) 277–283.
[64] W. Setyawan, G. Nandipati, K.J. Roche, H.L. Heinisch, B.D. Wirth, R.J. Kurtz, Displacement cascades and defects annealing in tungsten, Part I: defect database from molecular dynamics simulations, J. Nucl. Mater. 462 (2015) 329–337.
[65] V. Sikka, J. Moteff, "Rafting" in neutron irradiated tungsten, J. Nucl. Mater. 46 (2) (1973) 217–219.
[66] M. Wen, N.M. Ghoniem*, B.N. Singh, Dislocation decoration and raft formation in irradiated materials, Phil. Mag. 85 (22) (2005) 2561–2580.
[67] C. Jiang, N. Swaminathan, J. Deng, D. Morgan, I. Szlufarska, Effect of grain boundary stresses on sink strength, Materials Research Letters 2 (2) (2014) 100–106.